ISSN 1674-1056
http://cpb.iphy.ac.cn
http://iopscience.iop.org/cpb
中国物理 B Chinese Physics
中国物理 Chinese Physics B

Microstructure evolution and passivation quality of hydrogenated amorphous silicon oxide (a-SiO_x:H) on <100> and <111>-orientated c-Si wafers

Jun-Fan Chen(陈俊帆), Sheng-Sheng Zhao(赵生盛), Ling-Ling Yan(延玲玲), Hui-Zhi Ren(任慧志), Can Han(韩灿), De-Kun Zhang(张德坤), Chang-Chun Wei(魏长春), Guang-Cai Wang(王广才), Guo-Fu Hou(侯国付), Ying Zhao(赵颖), Xiao-Dan Zhang(张晓丹)

Citation: Chin. Phys. B . 2020, 29(3): 038801 . **doi:** 10.1088/1674-1056/ab6c47
Journal homepage: http://cpb.iphy.ac.cn; http://iopscience.iop.org/cpb

What follows is a list of articles you may be interested in

Designing solar-cell absorber materials through computational high-throughput screening

Xiaowei Jiang(江小蔚), Wan-Jian Yin(尹万健)
Chin. Phys. B . 2020, 29(2): 028803 . **doi:** 10.1088/1674-1056/ab6655

Analysis of highly efficient perovskite solar cells with inorganic hole transport material

I Kabir, S A Mahmood
Chin. Phys. B . 2019, 28(12): 128801 . **doi:** 10.1088/1674-1056/ab520f

Effect of carrier mobility on performance of perovskite solar cells

Yi-Fan Gu(顾一帆), Hui-Jing Du(杜会静), Nan-Nan Li(李楠楠), Lei Yang(杨蕾), Chun-Yu Zhou(周春宇)
Chin. Phys. B . 2019, 28(4): 048802 . **doi:** 10.1088/1674-1056/28/4/048802

Insight into band alignment of Zn(O,S)/CZTSe solar cell by simulation

Zhen-Wu Jiang(姜振武), Shou-Shuai Gao(高守帅), Si-Yu Wang(王思宇), Dong-Xiao Wang(王东潇), Peng Gao(高鹏), Qiang Sun(孙强), Zhi-Qiang Zhou(周志强), Wei Liu(刘玮), Yun Sun(孙云), Yi Zhang(张毅)
Chin. Phys. B . 2019, 28(4): 048801 . **doi:** 10.1088/1674-1056/28/4/048801

Influence of interface states, conduction band offset, and front contact on the performance of a-SiC: H(n)/c-Si(p) heterojunction solar cells

Zhi Qiao(乔治), Jian-Li Ji(冀建利), Yan-Li Zhang(张彦立), Hu Liu(刘虎), Tong-Kai Li(李同锴)
Chin. Phys. B . 2017, 26(6): 068802 . **doi:** 10.1088/1674-1056/26/6/068802

Microstructure evolution and passivation quality of hydrogenated amorphous silicon oxide (a-SiO_x:H) on ⟨100⟩- and ⟨111⟩-orientated c-Si wafers*

Jun-Fan Chen(陈俊帆)[1,2,3,4,†], Sheng-Sheng Zhao(赵生盛)[1,2,3,4,†], Ling-Ling Yan(延玲玲)[1,2,3,4], Hui-Zhi Ren(任慧志)[1,2,3,4], Can Han(韩灿)[1,2,3,4], De-Kun Zhang(张德坤)[1,2,3,4], Chang-Chun Wei(魏长春)[1,2,3,4], Guang-Cai Wang(王广才)[1,2,3,4,‡], Guo-Fu Hou(侯国付)[1,2,3,4,§], Ying Zhao(赵颖)[1,2,3,4], and Xiao-Dan Zhang(张晓丹)[1,2,3,4]

[1] *Institute of Photoelectronic Thin Film Devices and Technology of Nankai University, Tianjin* 300350, *China*
[2] *Key Laboratory of Photoelectronic Thin Film Devices and Technology of Tianjin, Tianjin* 300350, *China*
[3] *Engineering Center of Thin Film Photoelectronic Technology of Ministry of Education, Tianjin* 300350, *China*
[4] *Sino-Euro Joint Research Center for Photovoltaic Power Generation of Tianjin, Tianjin* 300350, *China*

(Received 14 November 2019; revised manuscript received 8 January 2020; accepted manuscript online 16 January 2020)

Hydrogenated amorphous silicon oxide (a-SiO_x:H) is an attractive passivation material to suppress epitaxial growth and reduce the parasitic absorption loss in silicon heterojunction (SHJ) solar cells. In this paper, a-SiO_x:H layers on different orientated c-Si substrates are fabricated. An optimal effective lifetime (τ_{eff}) of 4743 μs and corresponding implied open-circuit voltage (iV_{oc}) of 724 mV are obtained on ⟨100⟩-orientated c-Si wafers. While τ_{eff} of 2429 μs and iV_{oc} of 699 mV are achieved on ⟨111⟩-orientated substrate. The FTIR and XPS results indicate that the a-SiO_x:H network consists of SiO_x (Si-rich), Si–OH, Si–O–SiH_x, $SiO_2 \equiv$ Si–Si, and $O_3 \equiv$ Si–Si. A passivation evolution mechanism is proposed to explain the different passivation results on different c-Si wafers. By modulating the a-SiO_x:H layer, the planar silicon heterojunction solar cell can achieve an efficiency of 18.15%.

Keywords: a-SiO_x:H, orientated wafers, silicon heterojunction

PACS: 88.40.H–, 84.60.Jt, 88.40.jj **DOI:** 10.1088/1674-1056/ab6c47

1. Introduction

Nowadays, silicon heterojunction (SHJ) solar cell has received much attention, due to its advantages of high performance, low cost, simple manufacturing, non-toxic, *etc*. Meanwhile, the word-record conversion efficiency of 26.63% has been achieved on SHJ.[1] As is well known, the remarkable passivation materials such as a-Si:H play a crucial role in SHJ devices, of which the open-circuit voltage (V_{oc}) value has reached up to 750 mV.[2–4] However, the SHJ solar cells suffer the parasitic absorption of a-Si:H layers, and thus reducing the short-circuit current density (J_{sc}) in solar cells. In addition, it is difficult to fabricate a-Si:H film with low optical gap, which can easily cause an epitaxial growth on c-Si substrate.[5] To avoid such a kind of loss, a-SiO_x:H layers offer an optimistic solution.

The development of a-SiO_x:H was derived from the technology in which a-Si:H is alloyed with oxygen, thus an increase in the optical gap was observed with increasing oxygen content (c_o), which leads the parasitic absorption losses to decrease.[6] On one hand, the alloyed oxygen can improve passivation quality of a-Si:H, which is mainly attributed to the manipulated defect density and suppressed epitaxial growth on c-Si substrate.[2,7–9] On the other hand, the exceeded oxygen might lead to inferior passivation quality in the presence of interconnected voids.[10] Thus, the pivotal to acquiring superior passivation quality is an appropriate value c_o. Therefore, the passivation quality is a rather complex quantity, influenced not only by the intrinsic properties of the layer, but also by the characteristics of the substrate. In this paper, a-SiO_x:H passivation layers with different thicknesses are investigated on ⟨100⟩- and ⟨111⟩-orientated c-Si wafers respectively, aiming to achieve better passivation quality on different substrates. Furthermore, the passivation mechanism and the microstructure evolution of a-SiO_x:H are analyzed by x-ray photoelectron spectroscopy (XPS) and reflect Fourier transform infrared (Re-FTIR) spectroscopy. Finally, the a-SiO_x:H layers are applied

*Project supported by the National Key Research and Deveopment Program of China (Grant No. 2018YFB1500402), the National Natural Science Foundation of China (Grant Nos. 61674084 and 61874167), the Fundamental Research Funds for Central Universities, China, the Natural Science Foundation of Tianjin City, China (Grant No. 17JCYBJC41400), the Open Fund of the Key Laboratory of Optical Information Science & Technology of Ministry of Education of China (Grant No. 2017KFKT014), the 111 Project, China (Grant No. B16027), the International Cooperation Base, China (Grant No. 2016D01025), and Tianjin International Joint Research and Development Center, China.

†These authors contributed equally to this work.
‡Corresponding author. E-mail: wgc2008@nankai.edu.cn
§Corresponding author. E-mail: gfhou@nankai.edu.cn

© 2020 Chinese Physical Society and IOP Publishing Ltd

to bifacial-polished silicon substrate for SHJ device fabrication.

2. Experimental details

The ⟨100⟩- and ⟨111⟩-orientated bifacial-polished floating-zone n-type c-Si wafers with resistivity values in a range of 1 Ω·cm–10 Ω·cm and a bulk lifetime of > 1000 μs were used. The c-Si wafers were cleaned by the standard RCA process followed by the cleaning with a 5% hydrofluoric acid (HF) solution to remove the native silicon oxide layer.[11] The a-SiO_x:H film was deposited on the bifacial side of the cleaned ⟨111⟩-orientated substrate by changing CO_2 flow, mixture gas pressure, and RF initial power. Then, the optimal deposition parameters were applied to the bifacial side of the cleaned ⟨100⟩ and ⟨111⟩ c-Si wafers with various film thicknesses.

To measure the τ_{eff} of the immersed HF silicon substrate and the passivation wafer, Sinton Instruments WCT-120 QSSPC tester was used in transient or quasi-steady state analysis mode of generalized (1/1) or (64/1) at an injection level of 1×10^{15} cm^{-3}.[12] The optical properties of the thin film sample were analyzed by measuring the transmission and reflection with a Varian–Cary 5000 spectrometer, including the Tauc optical bandgap and refractive index. For the FTIR measurements, a Thermo Scientific Nicolet iS10 spectrometer was used in reflection mode in a spectral range of 400 cm^{-1}–4000 cm^{-1}. The FTIR spectrum was universally used to obtain the information about the a-Si:H[13–16] and a-SiO_x:H[17,18] layers. In this paper, we mainly acquired the hydrogen and oxygen content from the FTIR spectrum measurement according to different peaks' wavenumbers for different absorbance values. For the Si–H bond, the stretching modes at 2000 cm^{-1}–2260 cm^{-1},[14,19,20] among which the stretching modes at 2085 cm^{-1}–2100 cm^{-1} originated from the stretching in $(SiH_2)_n$ or micro voids,[14] and stretching modes at 2140 cm^{-1}–2260 cm^{-1} came from the stretching in H-Si(Si_xO_y) ($x=0,1$; $y=1,2,3$).[17–20] For the Si–O–Si bond, the stretching modes at 940 cm^{-1}–1150 cm^{-1} were from the stretching in Si–O–Si–Si_yO_z ($y=1$; $z=0,1,2$).[18–20] The simulation fitting peaks were mainly split into several peaks at 900 cm^{-1}–1200 cm^{-1} and 1850 cm^{-1}–2300 cm^{-1}. In addition, the oxygen content (c_o) was estimated from the XPS spectrum in the passivated layer according to the peaks of Si^{+x} ($x=1$, 2, 3, 4) shown in the XPS spectrum.[21–24] In terms of the chemical bonding and energetic data, we could further obtain the growth mechanism of a-SiO_x:H from XPS spectra with various passivation layer thickness, and build a growth model of passivation layer.[25]

Finally, the optimized passivation condition was applied to the bifacial side of the cleaned substrate for fabricating the planar SHJ solar cell. The structure is schematically depicted in Fig. 1, which was constructed with Al/Ag front grid/ITO/P-type emitter layer/i-a-SiO_x:H/N-Fz-Si/i-a-SiO_x:H/N-type layer/Al back contact. All of the thin film silicon alloy layers were deposited in the PECVD system with various gas mixtures. Then, the ITO layer, metal grids, and back all-metal contact were made by the thermal evaporation. The solar cell area of 0.53 cm^2 was defined by the shadow mask for ITO deposition. Through a shadow mask (active area = 0.53 cm^2), thermally evaporated silver grids were deposited on the front side, and full area aluminum was deposited on the rear side. The solar cell performance was characterized by the current density *versus* voltage (*J*–*V*) measurements under an AM1.5 solar simulator (WXS-156S-L2, AM1.5GMM) with 100 mW/cm^2 at 25 °C. The external quantum efficiency (EQE) spectra were measured by using a QEX10 PV system, and the short-circuit current density (J_{sc}) was calculated by the integral of measured EQE and the AM1.5 solar spectrum.

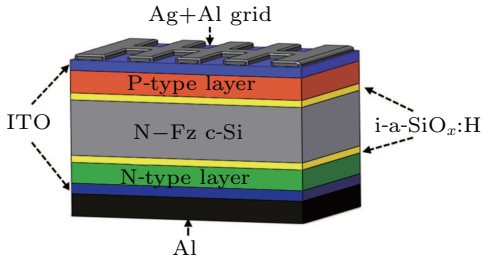


Fig. 1. Schematic diagram of planar SHJ solar cell fabricated with N–Fz c-Si wafer.

3. Results and discussion

3.1. Growth evolution model of a-SiO_x:H layer

In RF plasma, SiH_4 can be dissociated into SiH_3 and H (formula (1)),[26] whereas electronic kinetic energy or collision of electrons with H_2 molecules dissociates the H_2 molecules into H atoms. Then, CO_2 would be collided with H atom, which might form CO and OH (formula (2)).[26]

$$\text{SiH}_4 \rightarrow \text{SiH}_3 + \text{H}, \tag{1}$$

$$\text{H}_2 \xrightarrow{\text{e}} \text{H}+\text{H}, \quad \text{CO}_2+\text{H} \rightarrow \text{CO}+\text{OH}. \tag{2}$$

Thus, the oxygen in a-SiO_x:H can be reasonably attributed to the OH bonded with other complex groups, which incorporates with dangling Si bonds on the c-Si surface, reacts with SiH_3, H and itself to form novel complex groups as follows:[27–29]

$$\text{Si}-+\text{OH} \rightarrow \text{Si}-\text{OH}, \tag{3}$$

$$\text{Si}-\text{OH}+\text{SiH}_3 \rightarrow \text{Si}-\text{O}-\text{SiH}_2 \xrightarrow{\text{OH}} \text{Si}-\text{O}-\text{SiH}, \tag{4}$$

$$\text{Si}-\text{OH} \xrightarrow{\text{OH/H}} \text{Si}-\text{O}- \xrightarrow{\text{SiH}_3}$$

$$\text{Si}-\text{O}-\text{SiH}_3 \xrightarrow{\text{H}} \text{Si}-\text{O}-\text{SiH}_2 \xrightarrow{\text{OH}} \text{Si}-\text{O}-\text{SiH}. \tag{5}$$

From formulas (1)–(5), the a-SiO_x:H processes could be divided into three steps. First, SiH_4, CO_2, and H_2 are dissociated into precursors to form SiH_3 and OH (formulas (1) and (2)). Then, the precursor OH reacts with dangling Si

bond or broken-weak-Si–Si bond to form Si–OH group (formula (3)).[27] Finally, Si–OH combines with SiH_3, OH, and H to form Si–O–SiH_x ($x = 1, 2, 3$) (formulas (4) and (5)). However, a small part of Si–OH may remain unchanged in the a-SiO_x:H film.

The X_O is defined as the ratio of CO_2 flow rate to SiH_4 flow rate as follows:

$$X_O = \frac{CO_2}{SiH_4}. \tag{6}$$

From formulas (1)–(5) it may follow that the more the X_O increases, the more the inserted flow CO_2 will be. It is due to the quantity of OH precursors increasing that first process reacts right through the corresponding formula (2), which enhances the content of oxygen within the film.

3.2. Effective lifetime and iV_{oc} of a-SiO_x:H layer on ⟨111⟩- and ⟨100⟩-orientated c-Si wafers

In this study, we deposit a-SiO_x:H films with various thicknesses on ⟨111⟩- and ⟨100⟩-orientated c-Si substrates, respectively. Then τ_{eff} and iV_{oc} of corresponding samples were measured and are shown in Fig. 2.

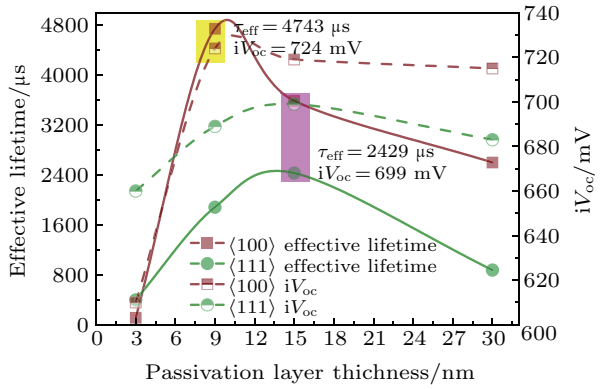


Fig. 2. The τ_{eff} and iV_{oc} of the a-SiO_x:H deposited on ⟨100⟩- and ⟨111⟩-orientated c-Si with various passivation layer thicknesses.

Figure 2 shows that τ_{eff} and iV_{oc} of a-SiO_x:H on the ⟨100⟩-orientated c-Si substrate first increase and thenc decrease with passivation layer thickness increasing. The optimal τ_{eff} and iV_{oc} values are achieved to be 4.74 ms and 724 mV on the 9-nm-thick a-SiO_x:H layer, respectively. If the passivation layer thickness is less than 9 nm, τ_{eff} and iV_{oc} of the corresponding samples show a growing trend with passivation thickness increasing. According to the descriptions mentioned above, the growth processes of a-SiO_x:H, OH, and H decomposed by SiH_4 continuously saturate the dangling Si bonds on the c-Si surface, resulting in the continuous reduction of surface defect states, thus improving the passivation quality of the samples. On the other hand, when the passivation layer thickness is higher than 9 nm, τ_{eff} and iV_{oc} of the passivated samples gradually decrease with passivation layer thickness increasing, probably caused by the increase of void microstructures by excessive OH precursors.[30] Additionally, excessive free H will also etch the film. Excessive OH may also rob the H atom from the passivation film and replaced it (generated Si–O–SiH_x, *etc.*), resulting in a decrease of total H content in the film and a trend of gradual decrease in passivation quality.

For the ⟨111⟩-orientated c-Si substrate, the τ_{eff} and iV_{oc} of the passivated samples show a trend of the extension with the inctrease of passivation thickness, indicating that the quantity of the precursors (OH and H) can fluctuate with the continuous introducing of CO_2, which further affects the content of O and H in the passivation material film. The passivation performances of a-SiO_x:H on the ⟨111⟩- and ⟨100⟩-orientated c-Si substrates present different rules, which probably relate to their corresponding c-Si surface microstructures.

3.3. Re-FTIR analysis of a-SiO_x:H

In order to analyze the process of a-SiO_x:H on the ⟨100⟩- and ⟨111⟩-orientated c-Si substrates, the FTIR spectroscopy is used to analyze the H and O contents in the film. For studying the thinner a-SiO_x:H, its Fourier transform infrared spectrum is measured by the reflected light signal. The result demonstrates that the Si–Si, Si–H, and Si–O–Si bonds may exist

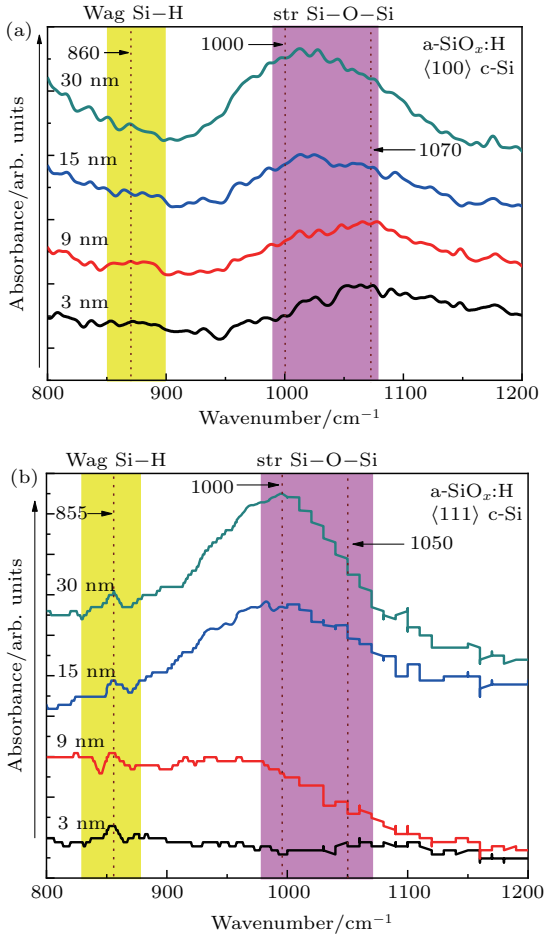


Fig. 3. FTIR spectra of a-SiO_x:H deposited on (a) ⟨100⟩- and (b) ⟨111⟩-orientated c-Si substrates with different passivation layer thicknesses.

in the a-SiO_x:H film. The feature signals of Si–H and Si–O in 800 cm^{-1}–1200 cm^{-1} and 1900 cm^{-1}–2300 cm^{-1} are corresponding to FTIR spectra on the ⟨100⟩- and ⟨111⟩-orientated c-Si substrates (see Figs. 3(a), 3(b), 4(a), and 4(b)).

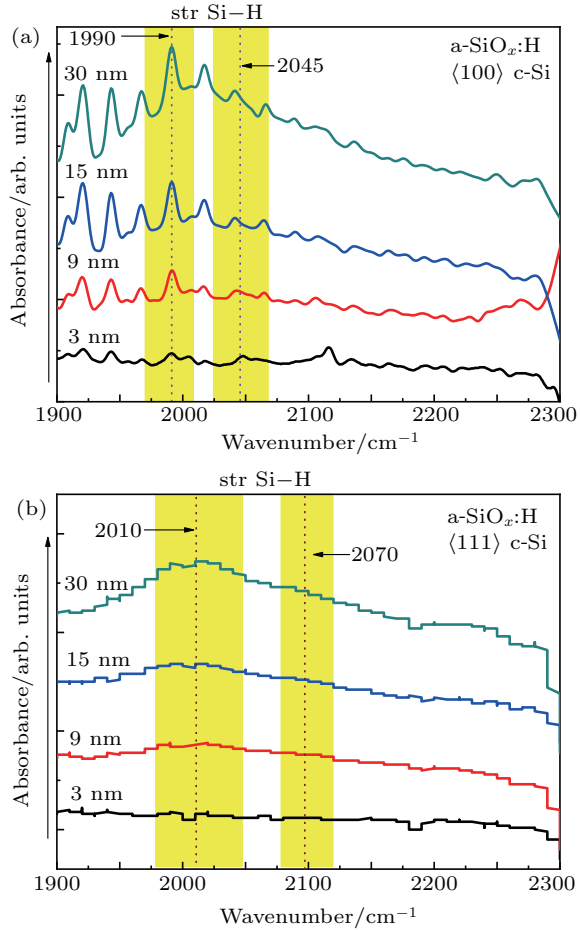


Fig. 4. FTIR spectra of a-SiO_x:H deposited on (a) ⟨100⟩- and (b) ⟨111⟩-orientated c-Si substrates with different passivation layer thicknesses.

From Fig. 3(a) it follows that the stretching vibrations of Si–O are raised at two peaks of 1000 cm^{-1} and 1070 cm^{-1} which correspond to Si–O–Si–Si_x (single-O) and (Si–O–Si)-SiO_x (O-rich), respectively. In addition, content of Si–O–Si–Si_x(O-rich) is higher than that of (Si–O–Si)–SiO_x (single-O) when the passivation layer thickness is less than 9 nm. It indicates that the O of introduced CO_2 is combined easily with Si to form (Si–O–Si)–SiO_x group with two phases of single-O and O-rich, that is, a-SiO_x:H contains the Si-rich and O-rich mixture component phases. The O atoms form mainly Si–O–SiH_x and Si–OH groups when the passivation layer thickness is 9 nm, the best a-SiO_x:H/c-Si interface passivation relates to higher content of hydrogen and perfect monohydride hydrogen termination.[31] With peaks moving from 1070 cm^{-1} to 1000 cm^{-1}, the content of (Si–O–Si)-SiO_x begins to increase after the passivation layer thickness has been larger than 9 nm, and more void microstructure in extended passivation layer thickness can be found, which leads to more defect density in the passivation sample. From Fig. 3(b), the stretching vibrations of Si–O occur at two peaks of 1000 cm^{-1} and 1050 cm^{-1}, which correspond to Si–O–Si–Si_x (single-O) and (Si–O–Si)–SiO_x (O-rich). The result further indicates that the a-SiO_x:H contains (Si–O–Si)–SiO_x group. In addition, as the thickness changes, the peak position remains basically constant, presumably the (111) c-Si surface suffered from an epitaxial interface of lower quality.[31]

From Fig. 4(a) it may follow that the FTIR spectrum of a-SiO_x:H deposited on the ⟨100⟩ and ⟨111⟩-orientated c-Si each shows two peaks of 1990 cm^{-1} and 2045 cm^{-1}, and 2010 cm^{-1} and 2095 cm^{-1} at 1900 cm^{-1}–2300 cm^{-1}, which correspond to the stretching vibration of Si–H with SiH_2 and Si–O–SiH_2 groups, respectively. Among them, the former peaks show stronger and increase rapidly, which results in the stretching vibration of Si–H mainly composed of SiH_2 group with passivation layer thickness increasing. Comparing with SiH_2 groups, the former peak is higher than the latter, which demonstrates that more hydrogen content can saturate the defects in the film microstructure, and thus verifying the trend of τ_{eff} and iV_{oc} on the ⟨100⟩-orientated c-Si as shown in Fig. 2.

3.4. XPS analysis

The oxygen content values of a-SiO_x:H on the ⟨100⟩- and ⟨111⟩-orientated c-Si substrates are valued by XPS technique. The binding energy scale is calibrated by assigning a value of 284.6 eV to the C 1s signal.[32] According to the relevant theoretical model,[25,33] peaks of Si–Si and Si–O bands are observed obviously on the XPS spectra of a-SiO_x:H films, respectively, deposited on ⟨100⟩-orientated Si 2p substrate (Fig. 5(a)) and ⟨111⟩-orientated Si 2p substrate (Fig. 6(a)). In addition, Si–H bond energy is far less than that of Si–O, which stably exists in the a-SiO_x:H film. Thus, silicon of passivation component is combined with oxygen, to form silicon oxides, which are divided into suboxide (SiO_x, $0 < x < 2$) and SiO_2. While the percentages of silicon oxygen took up in silicon compound, obtained from XPS are shown in Fig. 5(b) (for the case of ⟨100⟩-orientated Si 2p substrate) and Fig. 6(b) (for the case of ⟨111⟩-orientated Si 2p substrate), respectively.

From Figs. 5(a) and 6(a) we can see that the characteristic peaks of Si 2p and Si–Si first increase and then decrease as passivation layer thickness increases. According to Figs. 5(b) and 6(b), content of silicon suboxide is less than that of SiO_2. When the passivation layer thickness is 9 nm, more silicon suboxides exist, and the content of Si–Si will decrease on the ⟨100⟩-orientated c-Si substrate. The result shows that the content of Si–O–SiH_3 group is higher than that of Si–O–SiH and Si–O–SiH_2 group. Higher content of hydrogen and perfect monohydride hydrogen passivate the surface, and thus achiev-

ing the best passivation result. This is consistent with the analysis of FTIR spectrum. Also, the presence of SiO_x is a vitial factor that affects the τ_{eff} of the sample. The more void microstructure of network space passivation material is formed with the introducing of oxygen, which leads to the trend of τ_{eff} decreasing after the passivation layer thickness has been larger than 9 nm. While the content of silicon suboxide is almost zero, which demonstrates that on the ⟨111⟩-orientated c-Si substrate, the growth of silicon suboxide is suppressed or it is converted into SiO_2 when the passivation layer thickness is 30 nm. Combining with growth process of a-SiO_x:H, the content of Si–O–SiH_x shows fluctuating trend with content of OH varying. When the passivation layer thickness values are 9 nm and 15 nm respectively on the ⟨100⟩- and ⟨111⟩-orientated c-Si substrates, the XPS of Si 2p is fitted according to XPSPEAK41 software as can be seen from Figs. 7(a) and 7(b).

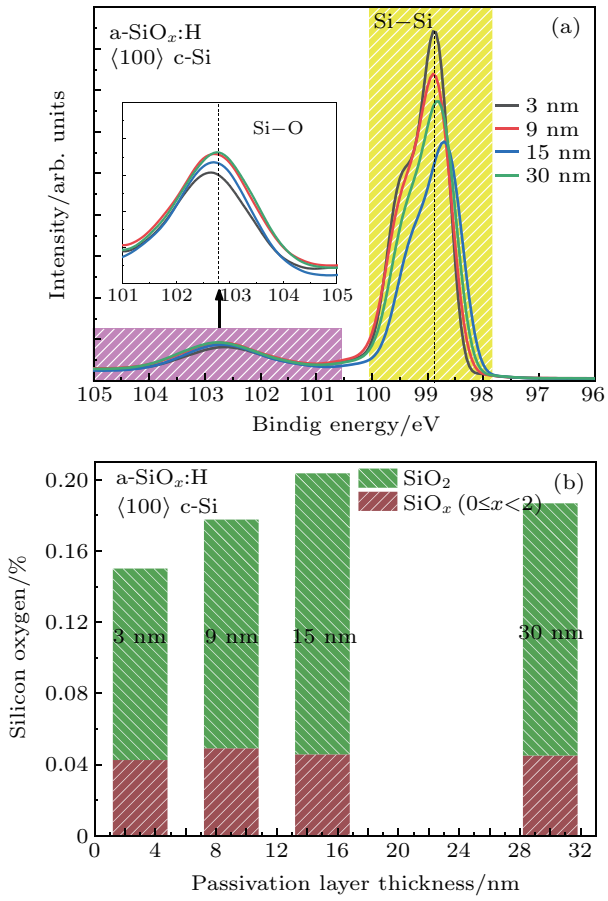


Fig. 5. (a) XPS of silicon and (b) percentage of silicon oxygen of a-SiO_x:H film deposited on the ⟨100⟩-orientated c-Si substrate with different passivation layer thicknesses.

The XPS peak of Si 2p can be decomposed into two peaks, that is, 2p3/2 and 2p1/2 peaks, and the area ratio of these two peaks is 2 : 1. According to the peak of 2p3/2, the chemical shifts of silicon oxides corresponding to Si^+, Si^{2+}, Si^{3+}, and Si^{4+} in their valence states are 0.86 eV, 1.5 eV, 2.4 eV, and 4.1 eV, respectively,[34] while the peak of 2p3/2 is at 98.86 eV. Figures 7(a) and 7(b) show that the content of SiO_2 is higher than that of SiO_x, and the percentage of Si is dominant in the two samples. It demonstates that Si from silicon oxide took up a small percentage, most of Si atoms exist in the form of Si–Si bond, which verifies the SiO_x (Si-rich) model, that is, the core of Si atom is surrounded by SiO_x with a certain network structure.[35] We can suppose that the content of Si^+ and Si^{2+} becomes more with chemical shifts of suboxide increasing. Stegemann *et al.*[36] pointed out that the growth of Si^{2+}oxide is suppressed at the interface of SiO_2/Si, so the content of Si^+ is most. In addition, we also identify the O groups by measuring XPS of O 1s to confirm the influence of OH and Si–O conten on passivation performance. According to the relevant literature,[37,38] the XPS of O 1s fitted three peaks (531.55 eV, 532.34 eV, and 533.1 eV) are, respectively, corresponding to C–O, Si–O, and OH groups obtained by XPSPEAK41 software, whose percentages of three groups are shown in Figs. 8 and 9. The C–O group comes from the organics attched to passivation material in the air, and is formed by reaction of CO_2 with H in PECVD.

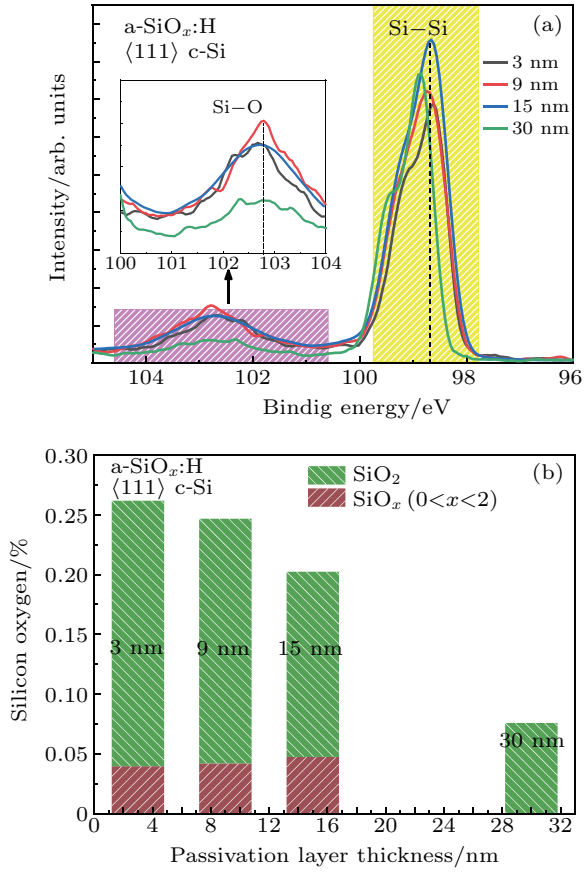


Fig. 6. (a) XPS of silicon and (b) percentage of silicon oxygen of a-SiO_x:H film deposited on the ⟨111⟩-orientated c-Si substrate with different passivation layer thicknesses.

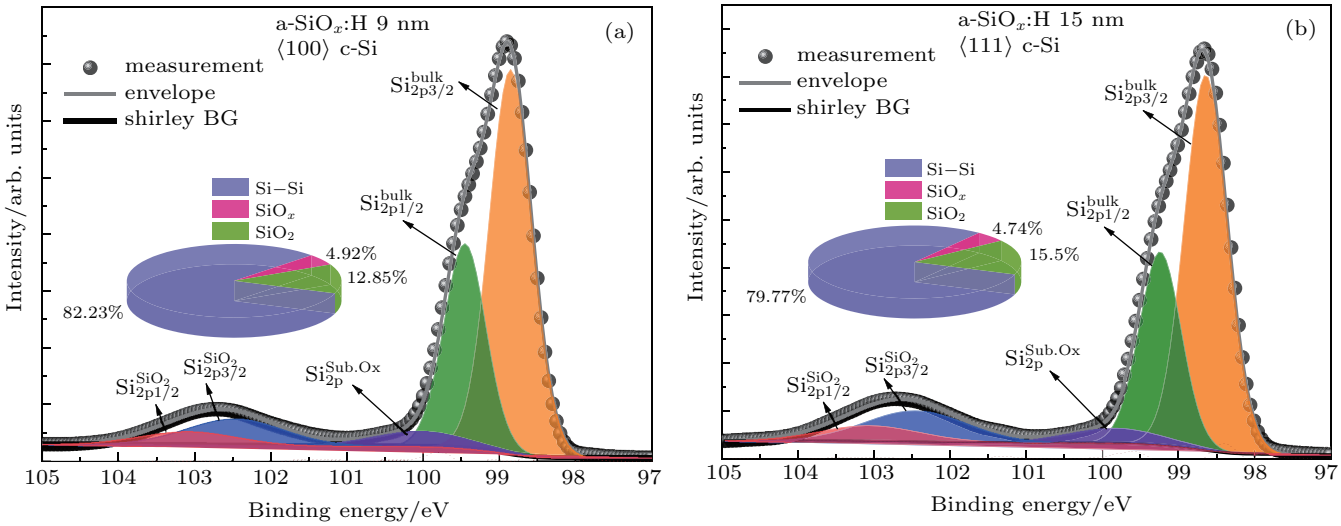


Fig. 7. XPS of Si 2p peaks fitted according to XPSPEAK41 software of a-SiO_x:H film deposited on the ⟨100⟩- and ⟨111⟩-orientated c-Si substrates with passivation layer thickness (a) 9 nm and (b) 15 nm.

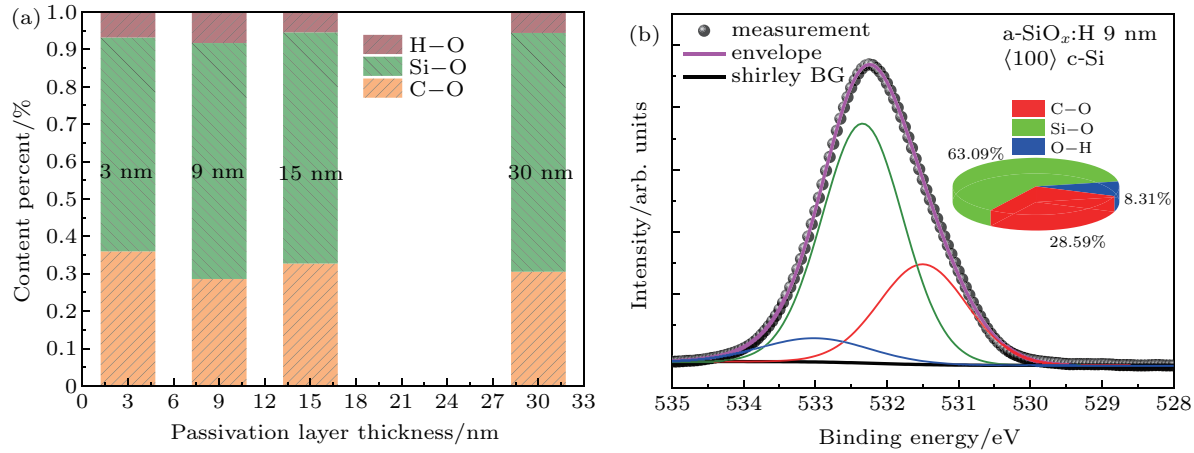


Fig. 8. (a) H–O, Si–O, and C–O percentages in XPS of O 1s with different passivation layer thicknesses and (b) 9-nm-thick passivation layer deposited on the ⟨100⟩-orientated c-Si substrate.

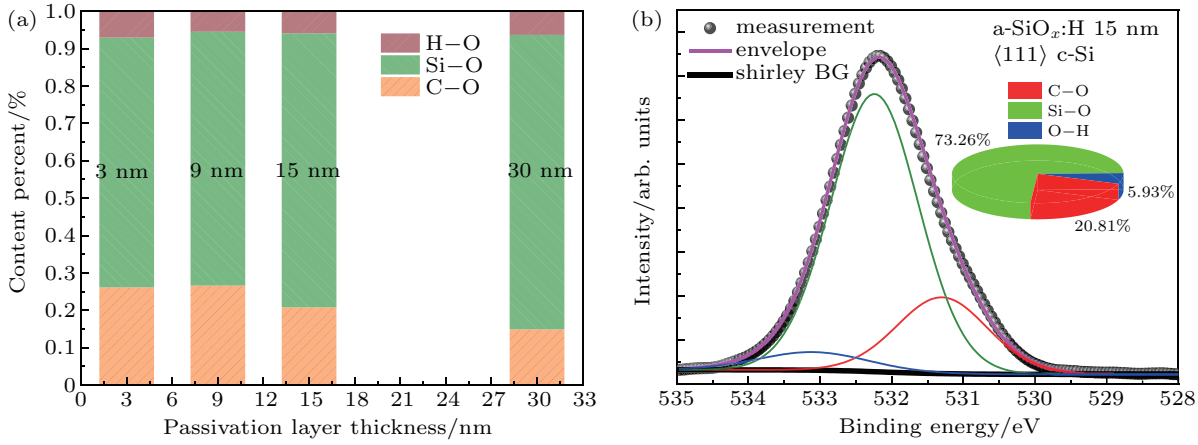


Fig. 9. (a) H–O, Si–O, and C–O percentages in XPS of O 1s with different passivation layer thicknesses and (b) 15-nm-thick passivation layer deposited on ⟨111⟩-orientated c-Si substrate.

From Fig. 8(a) it may follow that the Si–O and OH contents in the film deposited on the ⟨100⟩-orientated c-Si substrate first increase and then decrease, which is the same as contents of Si–O group in the film deposited on the ⟨111⟩-orientated c-Si substrate in Fig. 9(a). Both of these values consist in the most Si–O content which further verifies the SiO_x model (Si-rich). According to the above growth of a-SiO_x:H, the OH content will increase and form Si–OH or Si–O–SiH_x

($x = 1, 2, 3$) most, among which part of Si–OH forms SiO_x with O replacing H before the thickness of passivation layer reaches 9 nm.[38] According to the analysis of the above XPS of Si 2p, Si^+ oxide is the main content in silicon suboxide ($x \leq 1$), so Si–O–SiH_x may form and (SiO_x model with Si-rich and O-rich) symmetrical structure. Thus, oxygen vacancy and dangling bond of a-SiO_x:H microstructure will increase more and the corresponding $\tau_{\rm eff}$ and i$V_{\rm oc}$ decrease after the thickness of passivation layer has reached 9 nm on the ⟨100⟩-orientated c-Si sustrate as shown in Fig. 8(b). To the ⟨111⟩-orientated c-Si substrate, the raised and symmetrical structure will result in the fluctuation of $\tau_{\rm eff}$ and i$V_{\rm oc}$. In addition, SiO_x (Si-rich) model is identified further from Figs. 8(b) and 9(b), which consists of a small number of Si–OH and Si–O–SiH_x complex groups.

In summary, the components of a-SiO_x:H film deposited on the ⟨100⟩- and ⟨111⟩-orientated c-Si substrates are identified by XPS analysis. The SiO_x network model with Si-rich a-SiO_x:H is comfirmed by XPS of Si 2p and O 1s which consists of Si–OH, Si–O–SiH_x, and rich in oxygen vaccury and dangling bond complex components. Comparing with ⟨100⟩-orientated c-Si substrate, the passivation quality of the ⟨111⟩-orientated c-Si substrate is better subjecte to the subsequent arising of and with passivation layer thickness increasing. And a-SiO_x:H is more suitable for passivating ⟨100⟩-orientated c-Si substrate.

3.5. a-SiO_x:H/c-Si silicon heterojunction solar cell

We prepare two kinds of passivation layers (a-Si:H and a-SiO_x:H) with different thicknesses, and apply them to SHJ solar cells. The results are shown in Fig. 10.

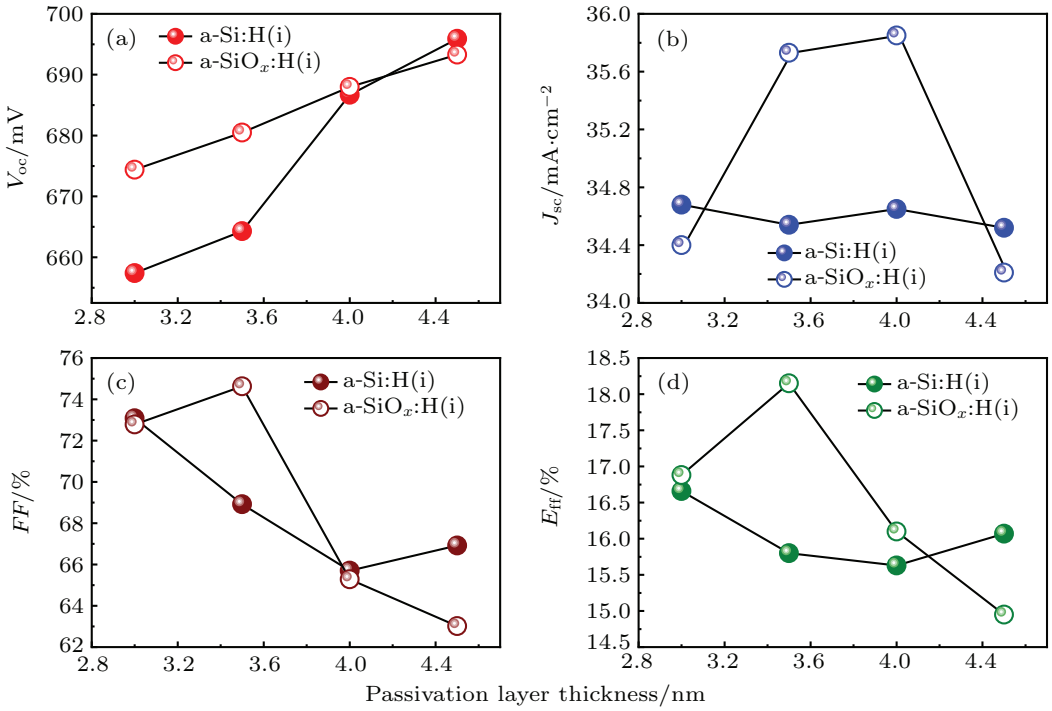


Fig. 10. The *J*–*V* parameters, (a) $V_{\rm oc}$, (b) $J_{\rm sc}$, (c) *FF*, and (d) $E_{\rm ff}$, of a-SiO_x:H/c-Si, a-Si:H/c-Si SHJ solar cells.

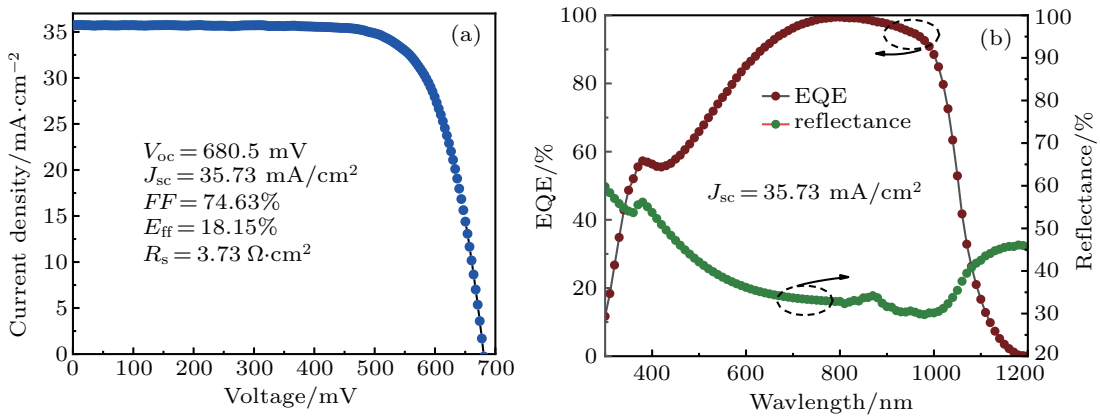


Fig. 11. (a) The *J*–*V* curve and (b) EQE/reflectance spectrum of the champion a-SiO_x:H/c-Si SHJ solar cell.

For a-Si:H and a-SiO_x:H passivation layer, as the thickness of the passivation layer increases, the V_{oc} of SHJ solar cells becomes higher. Besides, as the thickness of the passivation layer is less than or equal to 4 nm, a-SiO_x:H is better than a-Si:H passivation layer. However, as the thickness of the passivation layer is thicker than 4 nm, the performance of a-Si:H passivation is better than that of a-SiO_x:H. The reason might be that the internal defect states of the a-SiO_x:H film may increase with passivation layer thickening, leading the passivation effect to degrade. In addition, the FF and J_{sc} are observed to decease with passivation layer thickness increasing. SHJ solar cells with a-Si:H and a-SiO_x:H passivation layers demonstrate conversion efficiencies of 16.88% and 18.15%, respectively. Due to much improved passivation effect of a-SiO_x:H, the performance of SHJ cells with a-SiO_x:H/c-Si structure is better than that of a-Si:H/c-Si.

With the mentioned model of a-SiO_x:H affecting passivation performance of c-Si with $\langle 100 \rangle$- and $\langle 111 \rangle$-orientated substrates, we use the optimal a-SiO_x:H on the SHJ solar cells to achieve excellent device with suitable thickness, which can achieve the excellent passivation performance with $\tau_{eff} =$ 2168 μs, thereby resulting in high V_{oc}. The passivation layer modifies the open potential and enhances the red light response of the SHJ solar cell. As shown in Fig. 11(b), from 600 nm to 800 nm the reflectance of a-SiO_x: H decreases, the optical transmittance increases, and the red light response is improved.

4. Conclusions

In this work, we investigate a-SiO_x:H films deposited on the $\langle 100 \rangle$- and $\langle 111 \rangle$-orientated c-Si substrates with various passivation layer thicknesses, which exhibit different passivation qualities. According to the FTIR and XPS analysis, we conclude that Si-rich network model of a-SiO_x:H consists of Si–OH, Si–O–SiH_x, and other complex components and then the passivation evolution mechanism is proposed. When the optimal a-SiO_x:H film is used as the passivation layer in the planar SHJ solar cell, an efficiency of 18.15% is achieved. This research may provide a useful guideline for further improving the performance of SHJ solar cells.

References

[1] Yoshikawa K, Yoshida W, Irie T, Kawasaki H, Konishi K, Ishibashi H, Asatani T, Adachi D, Kanematsu M and Uzu H 2017 *Sol. Energy Mater. Sol. Cells* **173** 37

[2] Fujiwara H, Kaneko T and Kondo M 2007 *Appl. Phys. Lett.* **91** 481

[3] Hamakawa Y, Fujimoto K, Okuda K, Kashima Y, Nonomura S and Okamoto H 1983 *Appl. Phys. Lett.* **43** 644

[4] Taguchi M, Yano A, Tohoda S, Matsuyama K, Nakamura Y, Nishiwaki T, Fujita K and Maruyama E 2014 *IEEE J. Photovoltaics* **4** 96

[5] Peter Seif J, Descoeudres A, Filipič M, Smole F, Topič M, Charles Holman Z, De Wolf S and Ballif C 2014 *J. Appl. Phys.* **115** 024502

[6] Ding K, Aeberhard U, Finger F and Rau U 2013 *J. Appl. Phys.* **113** 871

[7] Zhang H, Nakada K, Miyajima S and Konagai M 2015 *Phys. Status Solidi - Rapid Res. Lett.* **9** 225

[8] Krajangsang T, Inthisang S, Sritharathikhun J, Hongsingthong A, Limmanee A, Kittisontirak S, Chinnavornrungsee P, Phatthanakun R and Sriprapha K 2017 *Thin Solid Films* **628** 107

[9] Ohdaira K, Oikawa T, Higashimine K and Matsumura H 2016 *Current Appl. Phys.* **16** 1026

[10] Beyer W 2000 *J. Non-Crystalline Solids* **266** 845

[11] Sonobe H, Sato A, Shimizu S, Matsui T, Kondo M and Matsuda A 2006 *Thin Solid Films* **502** 306

[12] Sinton R A, Cuevas A and Stuckings M 2006 *IEEE Photovoltaic Specialists Conference*

[13] Knights J C, Lucovsky G and Nemanich R J 1978 *Phil. Mag. B* **37** 467

[14] Lucovsky G, Nemanich R J and Knights J C 1979 *Phys. Rev. B* **19** 2064

[15] Wagner H and Beyer W 1983 *Solid State Commun.* **48** 585

[16] Smets A H M, Kessels W M M, Van d S, M C M 2003 *Appl. Phys. Lett.* **82** 1547

[17] Lucovsky G and Pollard W B 1983 *J. Vac. Sci. Technol. A* **1** 313

[18] Lucovsky G, Yang J, Chao S S, Tyler J E and Czubatyj W 1983 *Phys. Rev. B* **28** 3225

[19] Samanta A and Das D 2009 *Sol. Energy Mater. Sol. Cells* **93** 588

[20] Babal P, Blanker J, Vasudevan R, Smets A H M and Zeman M *Photovoltaic Specialists Conference*

[21] Hübner K 1977 *Phys. Status Solidi* **42** 501

[22] Hübner K and Lehmann A 1978 *Phys. Status Solidi* **46** 451

[23] Engelke R, Roy T, Neumann H G and Hübner K 1981 *Phys. Status Solidi* **65** 271

[24] Hübner K 1977 *Phys. Status Solidi* **40** 133

[25] Temkin R J 1975 *J. Non-Crystalline Solids* **17** 215

[26] Kushner M J 1988 *J. Appl. Phys.* **63** 2532

[27] Smith F and Yin Z 1991 *J. Non-crystalline Solids* **137** 871

[28] Guizot J L, Nomoto K and Matsuda A 1991 *Surf. Sci.* **244** 22

[29] Kawasaki H, Ohkura H, Fukuzawa T, Shiratani M, Watanabe Y, Yamamoto Y, Suganuma S, Hori M and Goto T 1997 *Jpn. J. Appl. Phys.* **36** 4985

[30] Babal P, Blanker J, Vasudevan R, Smets A and Zeman M 2012 38*th IEEE Photovoltaic Specialists Conference* pp. 000321–000326

[31] Olibet S, Vallat-Sauvain E, Fesquet L, Monachon C, Hessler-Wyser A, Damon-Lacoste J, De Wolf S and Ballif C 2010 **207** 651

[32] Marr G V 2013 *Handbook on Synchrotron Radiation: Vacuum Ultraviolet and Soft X-ray Processes*, Vol. 2 (New York: Elsevier)

[33] Schaefer J A, Stucki F, Frankel D J and Gopel W 1984 *J. Vac. Sci. Technol. B* **2** 359

[34] Richter S, Kai K, Naumann V, Werner M, Graff A, Gro?er S, Moldovan A, Zimmer M, Rentsch J and Bagdahn J 2015 *Sol. Energy Mater. Sol. Cells* **142** 128

[35] Samanta S and Das D 2018 *Physica E* **103** 99

[36] Stegemann B, Gad K M, Balamou P, Sixtensson D, Vössing D, Kasemann M and Angermann H 2017 *Appl. Surf. Sci.* **395** 78

[37] Mehonic A, Buckwell M, Montesi L, Garnett L, Hudziak S, Fearn S, Chater R, Mcphail D and Kenyon A J 2015 *J. Appl. Phys.* **117** 833

[38] Krywko-Cendrowska A, Marot L, Steiner R, Mathys D, Meyer E and Szklarczyk M 2019 *J. Electroanal. Chem.* **832** 311

[39] Allen T G, Bullock J, Yang X, Javey A and De Wolf S 2019 *Nature Energy* **1** 15